Computation of Three-Dimensional Complex Flows

Proceedings of the IMACS-COST Conference on Computational Fluid Dynamics Lausanne, September 13–15, 1995

Edited by
Michel Deville, Spyros Gavrilakis, and Inge L. Ryhming

Notes on Numerical Fluid Mechanics, Volume 53
(Vieweg, Braunschweig 1996)

The title of the book series is allowed to be abbreviated as NNFM.

Numerical prediction of three–dimensional thermally driven flows in a rotating frame

S. Ahmed[1], B. G. Sherlock[2] and Q. G. Rayer[3]
(1) Department of Computer Science, Parks College of Saint Louis University, 500 Falling Springs Road, Cahokia, Illinois, 62206, USA
(2) Department of Electrical Engineering, University of Bath, Bath, UK
(3) Nuclear Electric Plc., Berkeley Technology Centre, Berkeley, Gloucestershire, GL13 9PB, UK

Abstract

An original approach has been used to solve the three–dimensional unsteady incompressible flow in a uniformly rotating frame. The governing equations of fluid motion are discretized using a control–volume procedure, which ensures the satisfaction of global conservation laws. Pressure and velocities are calculated iteratively at each time–level, yielding a semi–implicit scheme. Buoyancy effects are included by using the Boussinesq approximation. The current form of the energy equation neglects the presence of internal energy point sources and sinks, viscous dissipation of energy and work done by the body force. The model is tested by using it to simulate the three–dimensional incompressible flow in a fluid annulus rotating with uniform angular velocity, with differential heating provided by maintaining the side–walls of the convection chamber at separate temperatures. Fluid heat transports obtained from the model agree well with those obtained from experimental measurement.

1 Introduction

Geophysical fluid systems exhibit complex three–dimensional motions due to the interaction of differential heating and the earth's rotation. The understanding of these systems is assisted by the study of flows in a differentially heated rotating fluid annulus (Figure 1), which shares rotational and thermal forcing with them, but has simple well–defined boundary conditions [1]. Interest in rotating systems with barriers [2] is motivated by systems where zonal flow is obstructed by topographical features.

This paper presents a rigorous approach towards the numerical simulation of thermally driven three–dimensional flows. The incompressible Navier–Stokes

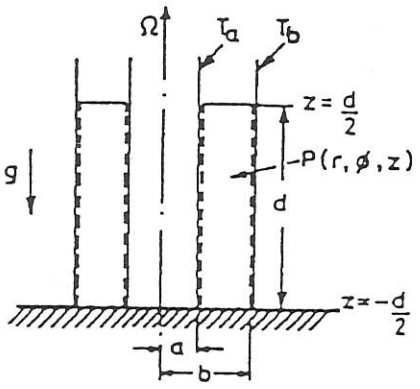

Figure 1 Diagram of fluid annulus. (r,ϕ,z) are cylindrical polar cordinates of a general point P, fixed in a frame rotating uniformly with the annulus at Ω rad. sec^{-1}. a=2.5cm, b=8.0cm, d=14cm.

equations in a rotating frame are solved, with buoyancy represented by the Boussinesq approximation. These governing equations are discretized using the control–volume approach [3, 4], thereby maintaining the statement of global conservation which is their essence. Preliminary results from this model have been presented [5], but the current paper extends them and gives a more detailed description of the model.

Previous computer models of the rotating fluid annulus have used grid–point finite–difference formulations which conserve mass, momentum and energy only in the limit as the simulation mesh becomes infinitely fine. They have been applied both to unobstructed flows [6, 7, 8] and to flows where the annulus is fully blocked by a thermally insulating radial barrier [2, 9]. The finite–difference model has so far failed to simulate several aspects of the flow in the annulus blocked by a radial barrier. Rayer [2] noticed defects in the velocity fields that may be similar to those mentioned by White [8]. Also the model did not calculate the correct value for the temperature drop observed across the thermally insulating barrier during experimental work. This may be due to an insufficiency of grid points adjacent to the barrier to adequately represent any boundary layer that may be present.

2 Computer Model

The new model uses the control–volume approach [3, 4]. The discretisation equation obtained by this method ensures that momentum and energy are exactly conserved over the computational domain. The physical variables of the system are expressed in non–dimensional terms for three–dimensional incompressible flow in a uniformly rotating frame. The reference velocity and characteristic time used for the non–dimensionalisation are

$$|\vec{\Omega}|\mathcal{L} = \omega\mathcal{L}, \text{ and } \frac{1}{|\vec{\Omega}|} = \frac{1}{\omega},$$

where $|\vec{\Omega}| = \omega$ and $\mathcal{L}$ is a characteristic length–scale. Then the non–dimensional variables become

$$\vec{x}^* = \frac{\vec{x}}{\mathcal{L}}, \quad \vec{u}^* = \frac{\vec{U}}{\omega\mathcal{L}}, \quad t^* = \omega t, \quad \mu^* = \frac{\mu}{\mu_0}, \quad \rho^* = \frac{\rho}{\rho_0}, \quad k^* = \frac{k}{k_0},$$

$$T^* = \frac{T - \mathcal{T}}{T_b - \mathcal{T}}, \quad \alpha^* = \alpha(T_b - \mathcal{T}), \quad p^* = \frac{p - \rho_0 g(d - z) - \frac{1}{2}\rho_0\omega^2 r^2}{\rho_0\omega^2\mathcal{L}^2}.$$

The parameters listed above are: position vector, $\vec{x} = (r, \phi, z)$; fluid veclcity, $\vec{u}^* = (u^*, v^*, w^*)$; reference fluid velocity, $\vec{U} = (\mathcal{U}, \mathcal{V}, \mathcal{W})$; time, t; fluid viscosity, μ; fluid density, ρ; thermal conductivity, k; temperature, T; mean fluid temperature, $\mathcal{T}$; pressure, p; thermal expansion coefficient, α and gravity, g. T_b is the temperature of the hot side–wall. With these definitions the differential operators become,

$$\frac{\partial}{\partial t} = \omega\frac{\partial}{\partial t^*}, \nabla = \frac{1}{\mathcal{L}}\nabla^*, \text{ where } \nabla^* = \hat{x}_i\frac{\partial}{\partial x_i^*}.$$

Thus using the Boussinesq approximation, the momentum conservation equations for three–dimensional incompressible baroclinic flow in a rotating frame can be written in non–dimensional form as

$$\frac{\partial\vec{u}^*}{\partial t^*} + \nabla^*.(\vec{u}^*\vec{u}^*) = -\nabla^* p^* + \mathrm{Gr}.\mathrm{Ro}^2 T^*\hat{z} - r^*\alpha^* T^*\hat{r} - 2u^*\hat{\phi} + 2\nu^*\hat{r} + \mathrm{Ro}\nabla^{*2}\vec{u}^*, \tag{2.1}$$

where Gr is the Grashoff number

$$\mathrm{Gr} = \frac{\rho_0^2 g\mathcal{L}^3\alpha(T_b - \mathcal{T})}{\mu_0^2},$$

and Ro is the Rossby number

$$\mathrm{Ro} = \frac{\mu_0}{\rho_0\omega\mathcal{L}^2}.$$

The energy equation becomes

$$\frac{\partial T^*}{\partial t^*} + (\vec{u}^*.\nabla^*)T^* = \frac{\mathrm{Ro}}{\mathrm{Pr}}\nabla^*.(k^*\nabla^* T^*),$$

where Pr is the Prandtl number,

$$\mathrm{Pr} = \frac{\mu_0 C_{P0}}{k_0}.$$

Equation (2.1) can be differenced in a control–volume manner with respect to the staggered grid and control–volume shown in Figure 2 to yield the discretised momentum conservation law, the r–component of which is

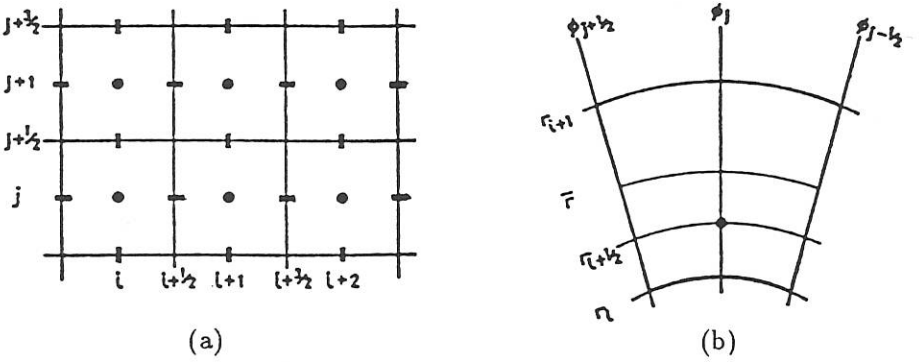

Figure 2 (a) Staggered grid used in control volume formulation. (b) Typical control-volume in (r,ϕ) plane.

$$\frac{u^{n+1}_{i+\frac{1}{2}}-u^{n}_{i+\frac{1}{2}}}{\Delta t}+\frac{[u_{i+1}u_{i+1}r_{i+1}-u_iu_ir_i]}{r_{i+\frac{1}{2}}\Delta r_{i+\frac{1}{2}}}+\frac{1}{r_{i+\frac{1}{2}}\Delta\phi_j}\left[(uv)_{i+\frac{1}{2},j+\frac{1}{2}}\cos(\phi_{j+\frac{1}{2}}-\phi_j)\right.$$
$$-(uv)_{i+\frac{1}{2},j-\frac{1}{2}}\cos(\phi_j-\phi_{j-\frac{1}{2}})-v^2_{i+\frac{1}{2},j+\frac{1}{2}}\sin(\phi_{j+\frac{1}{2}}-\phi_j)$$
$$\left.-v^2_{i+\frac{1}{2},j-\frac{1}{2}}\sin(\phi_j-\phi_{j-\frac{1}{2}})\right]+\frac{1}{\Delta z_k}\left[(uw)_{i+\frac{1}{2},k+\frac{1}{2}}-(uw)_{i+\frac{1}{2},k-\frac{1}{2}}\right]=$$
$$\mathrm{Ro}\left\{\frac{(u_{i+\frac{3}{2}}-u_{i+\frac{1}{2}})r_{i+1}}{\bar{r}\Delta r_{i+\frac{1}{2}}\Delta r_{i+1}}-\frac{(u_{i+\frac{1}{2}}-u_{i-\frac{1}{2}})r_i}{\bar{r}\Delta r_{i+\frac{1}{2}}\Delta r_i}+\frac{u_{i+\frac{1}{2},j+1}\cos(\phi_{j+1}-\phi_j)-u_{i+\frac{1}{2}}}{\bar{r}r_{i+\frac{1}{2}}\Delta\phi_j\Delta\phi_{j+\frac{1}{2}}}\right.$$
$$+\frac{u_{i+\frac{1}{2}}-u_{i+\frac{1}{2},j-1}\cos(\phi_j-\phi_{j-1})}{\bar{r}r_{i+\frac{1}{2}}\Delta\phi_j\Delta\phi_{j-\frac{1}{2}}}-\frac{u_{i+\frac{1}{2},j+1}\sin(\phi_{j+1}-\phi_j)}{\bar{r}r_{i+\frac{1}{2}}\Delta\phi_j\Delta\phi_{j+\frac{1}{2}}}$$
$$\left.+\frac{u_{i+\frac{1}{2},j-1}\sin(\phi_j-\phi_{j-1})}{\bar{r}r_{i+\frac{1}{2}}\Delta\phi_j\Delta\phi_{j-\frac{1}{2}}}+\frac{u_{i+\frac{1}{2},k+1}-u_{i+\frac{1}{2}}}{\Delta z_k\Delta z_{k+\frac{1}{2}}}-\frac{u_{i+\frac{1}{2},k}-u_{i+\frac{1}{2},k-1}}{\Delta z_k\Delta z_{k-\frac{1}{2}}}\right\}.$$

The fluxes at each cell face are calculated by upwind approximation. Discretization equations for the other flow variables are obtained similarly. The numerical scheme proceeds by first calculating u, v and w at the $n+1$ time–level explicitly from the momentum equations. However, this solution will not in general satisfy the continuity equation. Following the approach of [3] a Poisson equation for pressure correction is solved,

$$\nabla^2 p' = -\frac{1}{A}\nabla.\vec{u},$$

where A is a fictitious time–interval, followed by a velocity correction

$$\vec{u}' = A\nabla p'.$$

The corrected velocities and pressures are used to construct new fluxes at the cell faces. Upon iteration, this process yields velocities at the $n+1$ time–level which satisfy both the momentum and mass continuity equations. Because of the iterative update of the fluxes, the scheme is semi–implicit. The newly calculated

velocity field is then used to solve the energy equation for the fluid temperature at time–level $n+1$ in an explicit manner. Marching in time continues until the changes in the flow variables are sufficiently small to indicate that the procedure has converged. This convergence indicates that the flow has reached a steady–state, although the scheme, as described, is also capable of modelling time–varying flows.

3 Results

Representative flow fields (Figure 3) have been simulated for an annulus blocked by a radial barrier, using $T_b - T_a = \Delta T = 4°C$ and $\Omega = 0.5 rad.sec^{-1}$. The plots are in the form of fluid velocity vectors plotted in the (r, z)–plane opposite the barrier (Figure 3a) and in the (r, ϕ)–plane at mid–depth in the fluid (Figure 3b). Figure 3(a) shows fluid rising by the hot outer cylinder and sinking by the cold inner cylinder, accompanied by radial inflow near the top of the convection chamber and radial outflow at the bottom. This aspect of the simulated flow is consistent with experimental observations, although the circulations in a horizontal plane (Figure 3b) differ somewhat from [2]. The results also show that vertical motions take place mainly in the side–wall boundary–layers, as would be expected by consideration of the Taylor–Proudman theorem [10], which predicts that vertical velocities should be inhibited in the body of the fluid.

Fluid heat transfer (Table 1) and temperature data (Table 2) have been calculated using $T_b - T_a = \Delta T = 10°C$ and $\Omega = 0.4 rad.sec^{-1}$, and $T_b - T_a = \Delta T = 4°C$ and $\Omega = 0.5 rad.sec^{-1}$. Table 1 shows values of the fluid heat transfer in terms of the Nusselt number

$$\mathrm{Nu} = \frac{\mathrm{H} \ln(b/a)}{2\pi k \, \Delta T \, d},$$

where H is the total fluid heat transport calculated in the model as the heat conduction through the inner cylinder at $r = a$. The three columns give Nu from the model calculations; experimental measurements for nearly equivalent cases ($\Delta T = 9.98°C$, $\Omega = 0.402 rad.sec^{-1}$ and $\Delta T = 4.03°C$ and $\Omega = 0.401$, $0.601 rad.sec^{-1}$) [2] and from a correlation for Nu [11] derived for a stationary annulus, $\mathrm{Nu} = (0.203 \pm 0.010)\mathrm{Ra}^{\frac{1}{4}}$ where Ra is the Rayleigh number,

$$\mathrm{Ra} = \frac{g\alpha \, \Delta T \, (b-a)^3}{\nu\kappa},$$

and ν and κ are the kinematic viscosity and thermometric conductivity for the fluid. The results show excellent agreement between the model and experimental measurements, and illustrate the result [12] that the barrier makes the fluid heat transport largely independent of Ω.

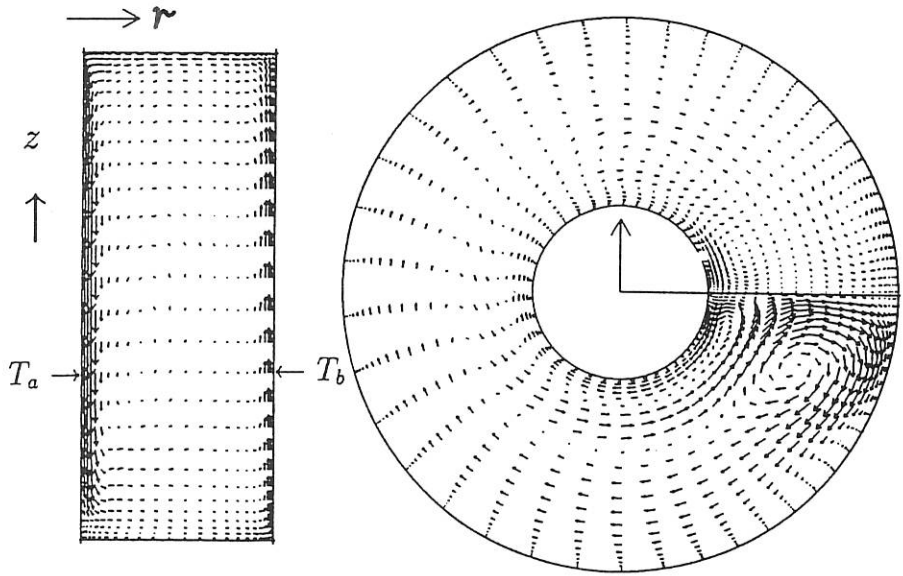

Figure 3 Fluid velocity vector plots, $\Delta T = 4°C$, $\Omega = 0.5$ rad. sec^{-1}, the scale arrow denotes a velocity of 1 cm. sec^{-1}. (a) Flow in the (r,z) plane opposite the radial barrier. (b) Flow in the (r,ϕ) plane at mid-depth in the annular chamber.

Table 1: Comparison of model and measurements of fluid heat transport.

ΔT °C	Ω $rad.sec^{-1}$	Nu *model*	Nu *expt [2]*	Nu($\Omega = 0$) *corrln [11]*
10	0.4	13.3	13.9 ± 0.1	13.6 ± 0.7
4	0.5	10.3	11.0 ± 0.2	10.8 ± 0.5

Table 2 shows the fluid temperature drop observed across the sides of the thermally insluating radial barrier at mid-height and mid-radius, ΔT_B. ΔT_B serves as a measure of the azimuthal temperature gradient in the fluid, and has been shown to be linked to the radial overturning cell observed in the blocked annulus [2]. The calculated values from the model have been compared with measurements [2]. It can be seen that although the calculated values of fluid heat transport agree quite closely with measurements, there is a considerable discrepancy between the calculated and measured values of ΔT_B. This indicates that the model is failing to properly reproduce the azimuthal temperature field in the annulus.

Table 2: Comparison of model and measurements of barrier temperature drop.

ΔT $^\circ C$	Ω $rad.sec^{-1}$	ΔT_B *model*	ΔT_B *expt [2]*
10	0.4	2.0	0.15 ± 0.01
4	0.5	0.7	0.17 ± 0.01

Bibliography

[1] R Hide (1977), Experiments with rotating fluids, Quart. J. Roy. Met. Soc., 103, 1–28.

[2] Q G Rayer (1992), An experimental investigation of heat transfer by large–scale motions in rotating fluids, D.Phil. thesis, Oxford University, UK.

[3] S V Patankar (1980), Numerical heat transfer and fluid flow, Hemisphere, ISBN 0891169199.

[4] D A Anderson, J C Tannehill and R H Pletcher (1984), Computational fluid mechanics and heat transfer, Hemisphere Pub Corp, New York, ISBN 0–89116–471–5.

[5] Q G Rayer, B G Sherlock and S Ahmed (1995), Simulation of the flow in a differentially heated rotating fluid, Syst. Anal. Modelling Simulation, Vol. 18–19, 149–152.

[6] I N James, P R Jonas and L Farnell (1981), A combined laboratory and numerical study of fully developed steady baroclinic waves in a cylindrical annulus, Quart. J. Roy. Met. Soc., 107, 51–78.

[7] P Hignett, A A White, R D Carter, W N D Jackson and R M Small (1985), A comparison of laboratory measurements and numerical simulations of baroclinic wave flows in a rotating cylindrical annulus, Quart. J. Roy. Met. Soc., 111, 131–154.

[8] A A White (1988), The dynamics of rotating fluids: numerical modelling of annulus flows. Met. Mag., 117, 54–63.

[9] Q G Rayer (1994), A numerical investigation of the flow in a fully blocked differentially heated rotating fluid annulus, Int. J. Modern Phys. C, Vol. 5, No. 2, 203–206.

[10] J Proudman (1916), On the motion of solids in a liquid possessing vorticity, proc. Roy. Soc. London A, 92, 408–424.

[11] M Bowden (1961), An experimental investigation of heat transfer in rotating fluids, Ph.D. thesis, University of Durham, UK.

[12] M Bowden and H F Eden (1968), Effect of a radial barrier on the convective flow in a rotating fluid annulus, J. Geophys. Res., 73, 6887–6896.

[13] W W Fowlis and R Hide (1965), Thermal convection in a rotating annulus of liquid: effect of viscosity on the transition between axisymmetric and non–axisymmetric flow regimes, J. Atmos. Sci., 22, 541–558.